

Rebalancing Modular Transit Systems: A Hierarchical Graph-Based Optimization Framework for Fleet Sizing and Routing

Tina Radvand, Alireza Talebpour*, Yanfeng Ouyang

The Grainger College of Engineering, Department of Civil & Environmental Engineering,
University of Illinois Urbana-Champaign, 205 N Mathews Ave, Urbana, IL 61801, USA

radvand2@illinois.edu, ataleb@illinois.edu, yfouyang@illinois.edu

Abstract. This study addresses the rebalancing of empty modular transit pods between scheduled service trips in fixed-route bus systems. A two-stage hierarchical optimization framework is proposed. The first stage determines the minimum fleet size and initial vehicle assignments by solving a maximum matching problem on a bipartite graph, using a GPU-accelerated push-relabel algorithm. The second stage formulates detailed routing as a series of minimum-cost flow problems on time-space networks. To manage memory usage in large instances, a capped-interval heuristic limits the size of each network by dividing long scheduling intervals into subintervals. Computational experiments on the Manhattan bus network show that the proposed method achieves performance comparable to the full-scale time-space network formulation in terms of objective value, while enabling the solution of instances that are otherwise intractable due to memory limitations.

1. INTRODUCTION

Public transit systems, especially bus services, are vital for sustainable urban development. They significantly help reduce road congestion (Stopher, 2004), reduce emissions (Bel and Holst, 2018), and provide fair access to transportation (Venter et al., 2018). However, putting these benefits into practice often faces many operational challenges.

In areas with low population density and low demand, traditional fixed-route bus services are often inefficient. They are fuel- and labor-intensive. This often leads transit agencies to cut service frequencies. Unfortunately, such cost-saving measures often cause ridership to drop even further, creating a negative cycle.

In contrast, busy urban areas struggle with peak-hour passenger overload (Tyrinopoulos and Antoniou, 2013) and longer travel times due to frequent stops (Ha et al., 2020). In addition, significant costs arise from moving empty buses to rebalance them for directional demand imbalances (Cortés et al., 2011).

Modular bus technology offers a promising alternative to conventional bus operations by addressing several of the aforementioned limitations. Its innovative design supports non-stop journeys (Khan and Menéndez, 2025), reducing overall travel times and minimizing service disruptions, such as bus bunching (Khan et al., 2023; Khan and Menéndez, 2023). In addition, modular buses can adjust available capacity according to demand, with more pods deployed during peak hours and fewer during off-peak periods. This flexibility helps maintain high fleet occupancy while ensuring the desired level of service (Tian et al., 2022; Cheng et al., 2024).

While modular transit offers considerable potential to address many current transit challenges, its effective implementation requires robust operational planning. This plan should specify the optimal number of pods in the fleet and cost-efficient strategies for routing them across a network to meet time-sensitive and fluctuating passenger demand.

Existing research on modular bus systems has primarily focused on optimizing operational parameters, such as headways and the number of pods assigned to each service trip (Dai et al., 2020). These studies concentrate on *in-service* routing, which addresses how modular pods are deployed to serve passengers. In contrast, *between-service* routing, i.e., the repositioning of empty pods across the network, has received little attention. For example, Pei et al. (2021) explicitly stated that they do not constrain fleet size, allowing them to dispatch “as many vehicles as necessary.” They also assumed unlimited parking capacity and deferred all cost-related considerations, including dwell time, acquisition, and maintenance, to a separate planning stage.

This study addresses this gap by proposing a framework for optimizing the routing of empty pods between service trips. Given the scheduled headways and pod capacities, the model determines cost-minimizing pod assignments while accounting for purchase, maintenance, parking, and repositioning costs. Accordingly, the

main contributions of this study to the literature on modular transit systems are (1) Introducing a binary linear optimization model to determine cost-efficient routing for rebalancing empty modular pods between scheduled service trips. This formulation provides the mechanism to capture pod acquisition, maintenance, parking, and repositioning costs within a fixed schedule with known demand. This approach captures costs associated with empty pod movements between services, a significant gap in the current literature; and (2) Introducing a novel two-step hierarchical solution approach capable of identifying the solution to the binary linear optimization model in an efficient and scalable manner. This method significantly reduces the complexity of the original problem by systematically breaking it into two stages: In the first step, the minimum fleet size is computed by reducing the problem to a minimum disjoint path cover in a directed acyclic graph (DAG). The advantage of this approach is that this graph-based representation can be transformed into a maximum matching problem on a bipartite graph and solved using an exact fast GPU-based push-relabel algorithm, ensuring scalability and efficiency of pod assignment to scheduled service trips in large transit networks. The second step aims to generate explicit routing plans by constructing time-space networks and solving a minimum-cost flow problem over the intervals between pod assignments. The flow in each of these time-space networks is a unit flow by construction. This knowledge allows the network to be broken into smaller, manageable pieces that can be solved sequentially to save memory and computing power. The computational performance, accuracy, and scalability of the aforementioned two-step hierarchical method is evaluated using real-world data from Manhattan bus transit network.

The remainder of this paper is organized as follows. Section 2 reviews related work. Section 3 presents the model formulation. Section 4 describes the solution approach, including integrated and hierarchical pod routing. Section 5 details the case study, covering data preparation, experimental design, and computational setup. Section 6 presents results and discussion, and Section 7 concludes the paper.

2. LITERATURE REVIEW

This section reviews selected literature on operational planning in modular transit systems, along with relevant fleet sizing and routing techniques.

Research in operational planning and management of modular transit has largely concentrated on optimizing in-service operations. These studies explore how modularity enhances service quality by adapting vehicle capacity and dispatching strategies to meet fluctuating demand. For instance, Dakic et al. (2021) developed a framework utilizing the three-dimensional macroscopic fundamental diagram (3D-MFD) to jointly determine the optimal composition of modular bus units and service frequency, aiming to enhance urban transit system efficiency. Similarly, Dai et al. (2020) proposed a dynamic programming approach to jointly optimize dispatch headways and vehicle capacities in a mixed traffic environment, minimizing total system cost.

Several studies also explored specific operational designs. Chen et al. (2019) focused on the operational design of shuttle systems with modular vehicles under oversaturated traffic, optimizing dispatch frequency, composition, and platooning decisions. Chen and Li (2021) proposed a discrete modeling method for designing transit corridor systems where modular autonomous vehicles adjust their formation dynamically at stations through docking and undocking operations. Pei et al. (2021) presented a mixed-integer nonlinear programming model for optimal vehicle dispatching and modular composition in a network, balancing vehicle operation costs and passenger trip time costs. Additionally, Cao and Zhao (2025) proposed an integer nonlinear programming (INLP) model that jointly optimizes departure intervals, modular vehicle capacity, short-turning schemes, and decoupling/coupling operations. The model explicitly accounts for modular units that are decoupled or coupled, deadheaded from, or returned to the depot.

While existing studies have significantly advanced our understanding of the benefits of utilizing modular transit for passenger service, their focus has been on optimizing in-service operations. They generally do not explicitly address the repositioning and scheduling of empty pods between service assignments. This is particularly critical to ensure cost-effective and smooth operations. Although crew scheduling has been widely studied in the transit literature (Muñoz, 2002) and shares some similarities with the between-service scheduling of modular pods, the two problems remain fundamentally different due to the constraints of human labor versus automated vehicle systems. This distinction leaves between-service routing in modular transit systems an underexplored gap in the current literature.

An important part of planning modular transit systems is finding the minimum fleet size. One established method in this area is presented by Ceder and Stern (1981). This approach involves a two-stage process: first, a graphical deficit function is used to determine an initial minimum number of vehicles for a fixed schedule. The second stage then systematically inserts deadheading trips to further reduce this fleet size, a procedure that is equivalent to solving maximum network flow. Building on this concept, Liu et al. (2020) adapted the deficit function theory to specifically address the minimum fleet size problem for autonomous modular public transit systems.

Another approach for finding the minimum fleet size in transportation systems is solving maximum matching on a bipartite graph (Bertossi et al., 1987). For example, Wang and Shen (2007) described a two-phase heuristic solution method for the Vehicle Scheduling Problem with Route and Fueling Time Constraints. The first phase generates vehicle rotations using a multiple ant colony algorithm. In the second phase, a bipartite graph model and an optimization algorithm are used to connect the rotations and minimize the number of vehicles deployed. The maximum matching of this bipartite graph is determined by computing the maximum inflow with the Ford–Fulkerson algorithm (Ford and Fulkerson, 2015). Zhan et al. (2016) proposed a foundational graph-theoretic approach that aimed to reduce the minimum fleet problem for taxi services to a maximum bipartite matching problem. Building on this, Vazifeh et al. (2018) applied this maximum bipartite matching approach to large-scale real-world taxi trip data to determine the minimum fleet size for on-demand urban mobility. Complementing these works, Ye and Shmoys (2023) provided a theoretical foundation by proving a min-max theorem for the minimum fleet size problem (i.e., the minimum fleet size needed equals the maximum number of pairwise incompatible trips), and demonstrated that this problem can be solved as a maximum bipartite matching.

In addition to finding the minimum fleet size, optimal scheduling in transit systems have been explored in the literature. Bus schedules are often optimized using minimum flow formulations in time-space networks. Klierer et al. (2006) studied the Multi-Depot Multi-Vehicle-Type Bus Scheduling Problem (MDVSP) to assign buses to cover timetabled trips, minimizing total costs, including fixed vehicle costs and variable operational costs (e.g., travel, idle time, empty movements, and waiting time). They utilized a time-space network model with node aggregation to reduce network size, solving instances with up to 7068 trips and 124 stations. More recently, Olsen et al. (2022) investigated flow decomposition methods for scheduling electric buses, also using aggregated time-space network models to determine and refine optimal vehicle rotations.

Unfortunately, even with node aggregation, time-space network-based solutions may become excessively large for modular transit networks. The variable number of pods (potentially, up to five pods) per bus runs significantly increases the complexity of the problem. Furthermore, real-world networks, such as Manhattan’s, can involve over 24,000 bus runs and approximately 1,900 bus stations, far exceeding the scale of instances solved by Klierer et al. (2006).

One effective way to tackle this complexity is through multi-stage heuristics that break down the problem into smaller, solvable components. For instance, Gintner et al. (2005) tackled the NP-hard multiple-depot, multiple-vehicle-type scheduling problem (MDVSP) using a two-phase “fix-and-optimize” heuristic. In the first phase, the original problem is decomposed into single-depot vehicle scheduling subproblems for each depot. These subproblems are solved, and common sequences of trips, referred to as “stable chains,” are identified. In the second phase, the stable chains are fixed in the original MDVSP formulation, which reduces the problem size and enables the computation of near-optimal solutions for large-scale instances. Similarly, Penna et al. (2019) proposed a hybrid metaheuristic (HILS-RVRP) for Rich Vehicle Routing Problems with Heterogeneous Fleets (HFRVRPs), which employs an implicit two-stage logic. The first stage generates initial solutions by assigning customers to vehicles and constructing preliminary routes via an insertion heuristic and the second stage iteratively refines these solutions through local search procedures and a set partitioning formulation that re-optimizes route-to-vehicle assignments.

Despite all these efforts in modular transit operational planning, a critical research gap persists. The current literature lacks a robust and scalable framework for the repositioning and scheduling of empty modular pods, considering all operational and capital costs, including those in between services. This study addresses this gap through introducing a scalable framework for modular pod rebalancing. The proposed framework formulates the public transit minimum fleet size problem as a maximum matching in a bipartite graph, that can be solved with a GPU-based model for enhanced efficiency. Moreover, this study introduces a hierarchical heuristic that

finds optimal pod routes by breaking the problem into small subproblems solvable in parallel on conventional compute platforms.

3. MODEL FORMULATION

This study addresses the problem of allocating modular transit pods within a fixed-route bus system to meet time-sensitive passenger demand. The system operates along multiple bus lines, each with a fixed sequence of station visits and arrival times. At each scheduled stop, a certain number of pods must be available to serve the passenger demand at that station. The objective is to determine the minimum fleet size and the routing of pods such that all service demands are met with the minimum operational cost.

To mathematically formulate the problem, we define the set of bus runs B , where each run $b \in B$ denotes a scheduled trip that visits an ordered sequence of stations at specified times. For each stop along a run, the required number of pods is known in advance based on the historical local passenger demand. We also assume that passengers can be moved freely across pods of the same bus run in between stops, so that excessive pods can be removed from the bus without disrupting service (Khan and Menéndez, 2025). For notational convenience, let $d_{s_i} \in \mathbb{Z}_+$ denote the number of pods required to serve demand at station s_i along the run. Figure 1 illustrates an example of four bus runs scheduled to address passenger demands within a bus transit network.

A pod’s movement includes two phases: (1) *In-service routing*, when the pod carries passengers along a bus run, and (2) *Between-service routing*, when the pod travels empty between runs. The details of pod routings for both phases are discussed in the following sections.

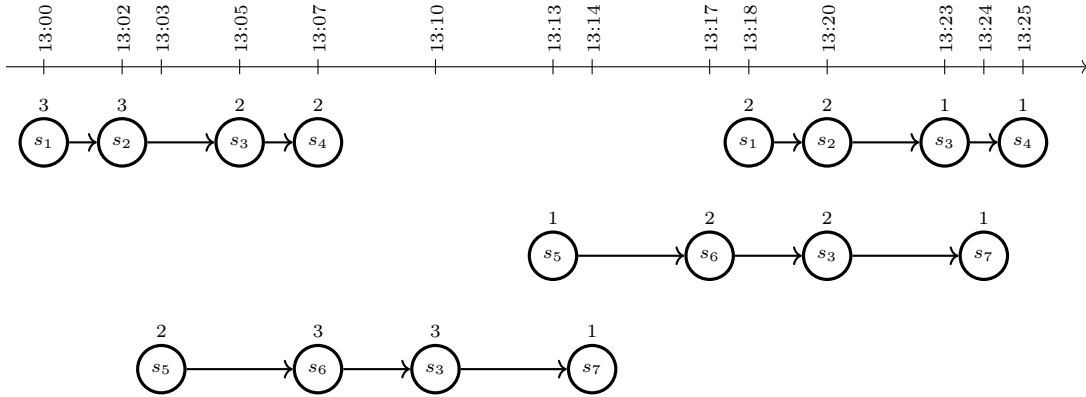


FIGURE 1. Illustration of a bus schedule within a bus network. Four bus runs operate to accommodate passenger demand, with the minimum number of required pods indicated above each station node. Nodes s_i correspond to stations in the network.

3.1. In-service routing. The in-service routing can be derived directly from the station-level passenger demand by decomposing each bus run into a set of pod routes. The detailed procedure is described in Algorithm 1. This decomposition ensures that no pod leaves the run before completing its passenger assignments. While the algorithm employs a greedy strategy, its optimality is proven in Theorem 1. An example of this decomposition is illustrated in Figure 2 for the runs presented in Figure 1.

Algorithm 1 decompose_bus_run

Input: Bus run b with ordered stations $[s_1, \dots, s_n]$, demands $\mathbf{d} = (d_{s_1}, \dots, d_{s_n})$ **Output:** Set of pod routes R $R \leftarrow \emptyset.$ **while** any $d_s > 0$ **do** Find first station s_i with $d_{s_i} > 0.$ Start new route r from $s_i.$ Extend r by adding consecutive s_j with $d_{s_j} > 0.$ Decrement d_s by 1 for all $s \in r.$ Add r to $R.$ **end while****return** R

Theorem 1. *Algorithm 1 returns the minimum number of pod routes required to serve the passenger demand.*

Proof. Given the bus run with demands $\mathbf{d} = (d_{s_1}, \dots, d_{s_n})$, the complete sequential multipartite graph $G = K_{d_{s_1}, d_{s_2}, \dots, d_{s_n}}$ is constructed. G includes one partition per station, with d_{s_i} nodes for partition i . Edges connect every pair of nodes in two consecutive non-empty partitions. A pod route is a path in G that visits consecutive nodes. A disjoint path cover is a set of such paths that are node-disjoint and together cover all nodes. The objective is to find a disjoint path cover of G with minimum cardinality, which corresponds to minimizing the number of pods required to serve the demand.

If $d_{s_i} = 0$ for any i , then G becomes disconnected into disjoint complete sequential multipartite subgraphs. Let H_1, \dots, H_m denote the resulting connected components. The minimum disjoint path cover of G is equal to the sum of the minimum disjoint path covers across all components. Hence, the proof may proceed by focusing on individual connected components. Let H be a connected component of G with $k \geq 1$ non-empty partitions.

Lemma 1. *There exists a minimum disjoint path cover of H that contains a path of length $k - 1$.*

Proof. The proof proceeds by induction on the size r of a minimum disjoint path cover in H .

Base case. For $r = 1$, all nodes are connected in a single path that includes one node from each of the k partitions, so the claim holds.

Inductive step. For $r \geq 2$, suppose the claim holds for all connected complete sequential multipartite graphs whose minimum disjoint path cover has size $r - 1$. Let H be a graph whose minimum disjoint path cover has size r . Let $\mathbf{P} = \{P_1, \dots, P_r\}$ denote an arbitrary minimum disjoint path cover of H . If some path $P_i \in \mathbf{P}$ already includes one node from each of the k partitions, the claim is satisfied. Otherwise, an arbitrary path from \mathbf{P} is selected and, without loss of generality, denoted by P_1 . Suppose P_1 begins at partition i . Since \mathbf{P} is a path cover of size $r \geq 2$, there exists another path that includes a node from a partition earlier than i . Another path that contains a node in a partition earlier than i is split at partition $i - 1$. Its initial segment is prepended to P_1 , and the resulting path remains node-disjoint from the others. A similar extension is applied at the end of P_1 by identifying a path with a node in a later partition, splitting it, and appending its tail to P_1 . By iteratively extending P_1 from both ends, a path is constructed that spans all k partitions. Each modification keeps the number of paths unchanged and ensures that each node belongs to exactly one path. Thus, the inductive claim is satisfied. \square

Returning to the full graph G , Algorithm 1 constructs such maximum-length paths iteratively. At each step, it selects the earliest unserved station and extends a path through all subsequent stations with available demand. This process corresponds exactly to identifying a longest path in one of the components H_i , removing it from the graph, and repeating the same operation on the residual graph. As shown above, such a longest path always exists in a minimum path cover. Therefore, Algorithm 1 returns a minimum disjoint path cover of G , and thus produces an exact solution. \square

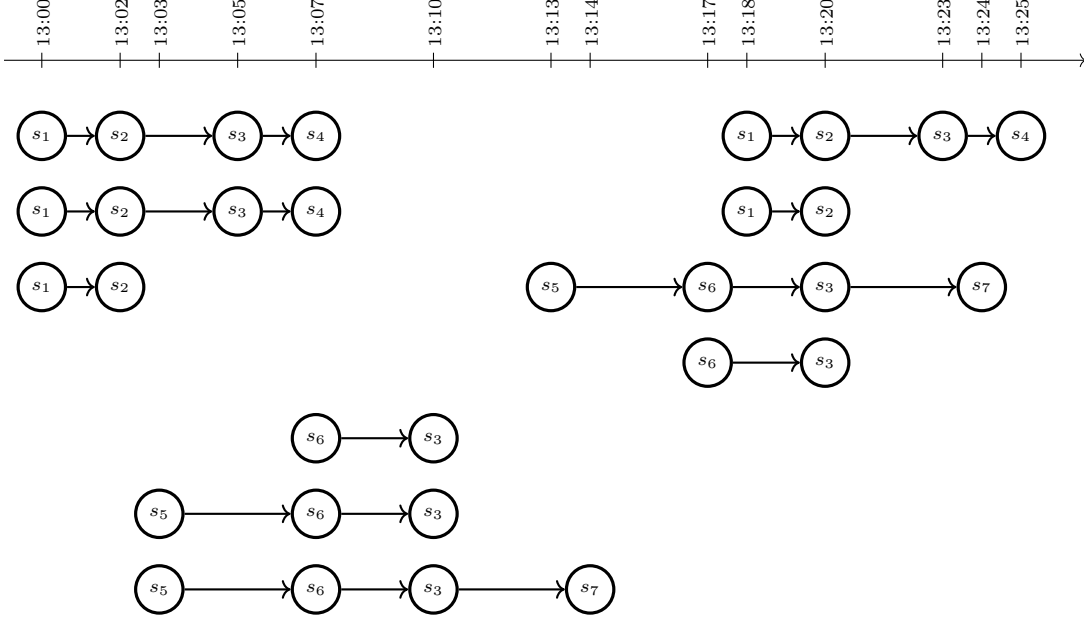


FIGURE 2. Decomposition of the bus runs shown in Figure 1 into individual pod routes. Each route represents the in-service journey of a single pod.

3.2. between-service routing. For between-service routing, the optimization model minimizes three types of cost. The first cost is a fixed fee per pod, c^{fleet} , charged for each service day. It covers the city’s capital investment in purchasing the pod, along with ongoing expenses such as maintenance, cleaning, and repairs. The second is a movement cost, c^{move} , applied per unit time when a pod travels empty between services. The third is a parking cost, c_s^{park} , charged per unit time when a pod is parked at station s . For simplicity, parking is assumed to be available near every station.¹ Because the in-service routes are fixed, their cost is a constant and is therefore not included in the optimization.

Table 1 summarizes the sets, indices, parameters, and decision variables used in the optimization model. While the model operates on a discrete time grid, route service is defined over continuous time. To align the two representations, the start and end times of each pod route are mapped to discrete time steps. For each route r , the continuous times StartTime_r and EndTime_r are mapped to discrete boundaries as follows:

$$t_r = \left\lfloor \frac{\text{StartTime}_r}{\Delta t} \right\rfloor \cdot \Delta t, \quad \bar{t}_r = \left\lceil \frac{\text{EndTime}_r}{\Delta t} \right\rceil \cdot \Delta t, \quad (1)$$

where t_r and \bar{t}_r are the earliest and latest discrete time steps that fully contain the route’s start and end, respectively.

Similarly, the continuous travel time $\tau_{s,s'}$ between stations s and s' is mapped to the discrete time grid by rounding it up to the nearest full time step. The resulting effective travel time, denoted by $\hat{\tau}_{s,s'}$, is given by:

$$\hat{\tau}_{s,s'} = \left\lceil \frac{\tau_{s,s'}}{\Delta t} \right\rceil \cdot \Delta t. \quad (2)$$

¹This assumption can be easily relaxed by introducing dedicated parking spaces in the network and adding deadheading costs. To keep the model straightforward, we do not pursue this extension here.

TABLE 1. Sets, indices, parameters, and decision variables

Sets and Indices	
S	Set of stations, indexed by $s \in \mathbf{S}$
B	Set of bus runs, indexed by $b \in \mathbf{B}$
K	Set of pods, indexed by $k \in \mathbf{K}$
T	Set of discrete time steps, $t \in \{0, 1, \dots, T_{\max}\}$
A	Set of directed arcs between distinct stations, i.e., $\mathbf{A} = \{(s, s') \in \mathbf{S} \times \mathbf{S} \mid s \neq s'\}$
R_b	Set of pod routes within bus run b , indexed by $r \in \mathbf{R}_b$
R	Set of all pod routes, $\mathbf{R} = \bigcup_{b \in \mathbf{B}} \mathbf{R}_b$
Parameters	
$d_{s,b}$	Number of pods required at station s in bus run b , $d_{s,b} \in \mathbb{Z}_+$
$\tau_{s,s'}$	Continuous travel time from station s to s' , $\tau_{s,s'} \in \mathbb{Z}_+$
Δt	Duration of each discrete time step
$\widehat{\tau}_{s,s'}$	Effective travel time: $\lceil \tau_{s,s'} / \Delta t \rceil \cdot \Delta t$
$\underline{t}_r, \bar{t}_r$	Discrete-time start and end bounds of pod route r
Start(r), End(r)	Start and end stations of pod route r
StartTime _{r} , EndTime _{r}	Continuous start and end times of pod route r
c^{fleet}	Fixed cost per pod per service day, $c^{\text{fleet}} \in \mathbb{R}_+$
c^{move}	Cost per unit time of empty repositioning, $c^{\text{move}} \in \mathbb{R}_+$
c_s^{park}	Cost per unit time of parking at station s , $c_s^{\text{park}} \in \mathbb{R}_+$
Decision Variables	
$x_{k,r}$	Binary, 1 if pod k serves pod route r , 0 otherwise, $x_{k,r} \in \{0, 1\}$
$y_{k,s,t}$	Binary, 1 if pod k is parked at station s at time t , 0 otherwise, $y_{k,s,t} \in \{0, 1\}$
$z_{k,s,s',t}$	Binary, 1 if pod k moves empty from station s to s' starting at time t , 0 otherwise, $z_{k,s,s',t} \in \{0, 1\}$
p_k	Binary, 1 if pod k is used, 0 otherwise, $p_k \in \{0, 1\}$

The resulting objective function is:

$$\begin{aligned}
\min \quad & c^{\text{fleet}} \sum_{k \in \mathbf{K}} p_k + c^{\text{move}} \sum_{k \in \mathbf{K}} \sum_{(s,s') \in \mathbf{A}} \sum_{t \in \mathbf{T}} \widehat{\tau}_{s,s'} \cdot z_{k,s,s',t} + \sum_{k \in \mathbf{K}} \sum_{s \in \mathbf{S}} \sum_{t \in \mathbf{T}} c_s^{\text{park}} \cdot y_{k,s,t} \\
& + \sum_{k \in \mathbf{K}} \sum_{r \in \mathbf{R}} x_{k,r} \cdot \left[(\text{StartTime}_r - \underline{t}_r) \cdot c_{\text{Start}(r)}^{\text{park}} + (\bar{t}_r - \text{EndTime}_r) \cdot c_{\text{End}(r)}^{\text{park}} \right] \quad (3)
\end{aligned}$$

The final term accounts for the discretization gap between the true route duration and its rounded service window. The early idle time ($\underline{t}_r - \text{StartTime}_r$) is charged as parking at the departure station, while the late idle time ($\bar{t}_r - \text{EndTime}_r$) is charged at the arrival station.

The model is subject to the following constraints.

(1) Route assignment: Each pod route must be served by exactly one pod to ensure full coverage of the demand. Formally, this is expressed as

$$\sum_{k \in \mathbf{K}} x_{k,r} = 1 \quad \forall r \in \mathbf{R}. \quad (4)$$

(2) Activity scheduling: Each active pod must be assigned to exactly one activity, i.e., serving a route, parked at a station, or moving empty between stations, at every time step. Since repositioning moves can span multiple discrete time steps, all those that may have started earlier and are still in progress must be considered. The constraints are:

$$\sum_{\substack{r \in \mathbf{R}: \\ t \in [\underline{t}_r, \bar{t}_r]}} x_{k,r} + \sum_{s \in \mathbf{S}} y_{k,s,t} + \sum_{\substack{(s,s') \in \mathbf{A}, t' \in \mathbf{T}: \\ t \in [t', t' + \widehat{\tau}_{s,s'}]}} z_{k,s,s',t'} = p_k \quad \forall k \in \mathbf{K}, t \in \mathbf{T}. \quad (5)$$

(3) Transition feasibility: To ensure realistic pod movements, each pod may begin an activity only if it is already present at the station at the corresponding time step. Presence at a station may result from being parked there previously, completing an empty trip to that station, or finishing a passenger-carrying route.

(a) *Feasibility of starting a route:* A pod may begin a route r at time t_r from station $\text{Start}(r)$ only if it is already there. As mentioned above, this condition is satisfied if the pod was parked at that station at the previous time step, had just arrived via empty movement, or had just completed another route that ends at that station and time:

$$x_{k,r} \leq y_{k,s,t-1} + \sum_{\substack{(s',s) \in \mathbf{A}, t' \in \mathbf{T}: \\ t=t'+\widehat{\tau}_{s',s}}} z_{k,s',s,t'} + \sum_{\substack{r' \in \mathbf{R}: \\ \text{End}(r')=s, \bar{t}_{r'}=t}} x_{k,r'} \quad \forall k \in \mathbf{K}, r \in \mathbf{R} : \text{Start}(r) = s, t_r = t > 0. \quad (6)$$

(b) *Feasibility of starting an empty movement:* A pod can only begin empty movement from station s at time t if it is already at s . This presence can result from being parked, arriving via an earlier move, or completing a route that ends at s at that time:

$$z_{k,s,s',t} \leq y_{k,s,t-1} + \sum_{\substack{(s'',s) \in \mathbf{A}, t' \in \mathbf{T}: \\ t=t'+\widehat{\tau}_{s'',s}}} z_{k,s'',s,t'} + \sum_{\substack{r \in \mathbf{R}: \\ \text{End}(r)=s, \bar{t}_r=t}} x_{k,r} \quad \forall k \in \mathbf{K}, (s,s') \in \mathbf{A}, t \in \mathbf{T} : t > 0. \quad (7)$$

(c) *Feasibility of parking:* A pod may be parked at station s at time $t > 0$ only if it was already there in the previous time step, or has just arrived via movement or completed a route at that time:

$$y_{k,s,t} \leq y_{k,s,t-1} + \sum_{\substack{(s',s) \in \mathbf{A}, t' \in \mathbf{T}: \\ t=t'+\widehat{\tau}_{s',s}}} z_{k,s',s,t'} + \sum_{\substack{r \in \mathbf{R}: \\ \text{End}(r)=s, \bar{t}_r=t}} x_{k,r} \quad \forall k \in \mathbf{K}, s \in \mathbf{S}, t \in \mathbf{T} : t > 0. \quad (8)$$

(5) Binary variables:

$$x_{k,r} \in \{0, 1\} \quad \forall k \in \mathbf{K}, r \in \mathbf{R}, \quad (9)$$

$$y_{k,s,t} \in \{0, 1\} \quad \forall k \in \mathbf{K}, s \in \mathbf{S}, t \in \mathbf{T}, \quad (10)$$

$$z_{k,s,s',t} \in \{0, 1\} \quad \forall k \in \mathbf{K}, (s,s') \in \mathbf{A}, t \in \mathbf{T}, \quad (11)$$

$$p_k \in \{0, 1\} \quad \forall k \in \mathbf{K}. \quad (12)$$

4. SOLUTION APPROACH

This section presents the methodologies developed to solve the modular pod rebalancing problem. Two distinct solution approaches are proposed: Integrated Pod Routing and Hierarchical Pod Routing. The Integrated Pod Routing approach formulates the problem on a time-space network, where the optimal solution is obtained by finding the minimum-cost flow. Individual pod paths are then retrieved by decomposing this flow. In contrast, the Hierarchical Pod Routing approach first assigns sequences of routes to pods by solving a minimum disjoint path cover problem on a Directed Acyclic Graph (DAG). Subsequently, the exact routes for empty pod movements between these assigned sequences are determined by solving minimum-cost flow problems on time-space networks tailored for the respective time intervals.

4.1. Integrated Pod Routing. The Integrated Pod Routing approach offers a framework for optimizing pod assignment, movement, and parking to minimize the total cost. This section discusses the underlying processes for constructing the time-space network, which spans the entire planning horizon. A discussion of its dimensions is also included.

The time-space network is constructed as a directed graph $G = (V, E)$. Figure 3 illustrates a simple bus transit schedule along with its corresponding network. To manage visual complexity but keeping a clear depiction of key elements, certain edges and nodes are shown with lower transparency. The network structure of vertices and edges is described below.

Vertices $v \in V$ are organized into several categories. Each vertex denotes a specific station at a discrete time step, and its category indicates whether a pod occupying that spatio-temporal point is in-service or between-service. Requester vertices are the spatio-temporal representation of the first station in a pod route. A pod at one of these vertices is in-service and begins its service segment. Requester vertices are illustrated with solid double blue circles in Figure 3b. Similarly, Releaser vertices are the spatio-temporal representation of the last station in a pod route. A pod at one of these vertices is in-service and concludes its service segment. Releaser vertices are illustrated with dashed red circles in Figure 3b. Middle vertices are the spatio-temporal representation of an intermediate station within an individual pod route. A pod at one of these vertices is in-service and maintains continuous service flow along its assigned segment. Middle vertices are illustrated with solid green circles in Figure 3b. To define the flow balance requirements, requester vertices are set to have a demand of one, as they need one pod. Conversely, Releaser vertices are set to have a supply of one, as they release one pod. Standby vertices are designated waiting and transfer areas within the network, intended for pods that are in an idle state. A standby vertex is created for each physical station at every discrete time interval, from which a pod can initiate parking or empty movement. Standby vertices are illustrated with dashed dot circles in Figure 3b. Finally, Auxiliary Vertices are introduced to complete the network's overall flow structure: A source vertex is added as the origin of all pod flow, and a sink vertex serves as the destination for all pod flow within the planning horizon. These are denoted by nodes S and T , respectively, in Figure 3b.

Edges represent possible transitions for a pod from one vertex to another, denoting a change in its location and time, or operational status. Each arc is associated with a specific cost. Each pod route, $r \in \mathbf{R}$, represents the in-service journey and consists of a sequence of vertices connected by edges that incur zero cost. The rest of the edges are categorized by the nature of the transition they represent.

For each pod route $r \in \mathbf{R}$, a Releaser-to-Standby edge connects the Releaser vertex at station $End(r)$ at time \bar{t}_r to the Standby vertex at the same station and time step. They represent a pod transitioning from an in-service state to a between-service state at a station. Each such edge is assigned a cost of $(\bar{t}_r - EndTime_r) \cdot c_{End(r)}^{park}$. This value accounts for the idle time created by mapping the route's continuous end time to the discrete time grid. These edges are shown with dashed arrows in Figure 3b. Similarly, for each pod route $r \in \mathbf{R}$, a Standby-to-Requester edge leaves the Standby vertex at station $Start(r)$ at time \underline{t}_r and goes to the Requester vertex for that same route r . They represent a pod transitioning from a between-service state to an in-service state to begin serving its assigned route. Each such edge is assigned a cost of $(StartTime_r - \underline{t}_r) \cdot c_{Start(r)}^{park}$. These edges are shown with dashed-dot arrows in Figure 3b.

Standby-to-Standby Movement edges represent empty pods traveling between different stations. From each standby vertex (s, t) , edges are established to standby vertices $(s', t + \hat{\tau}_{s,s'})$ for all other stations $s' \in \mathbf{S}$, $s' \neq s$, denoting the quickest possible travel from s to s' . They incur a cost of $c^{move} \cdot \hat{\tau}_{s,s'}$. Two standby-to-standby movement edges are highlighted in purple in Figure 3b. To keep the figure simple, edges between stations s_1 and s_3 are not shown. Standby-to-Standby Parking edges represent empty pods parking at the same station. An edge connects a standby vertex (s, t) to a standby vertex at the same station in the next time interval, $(s, t + 1)$. These edges have a cost of $c_s^{Park} \cdot \Delta t$. An standby-to-standby parking edge is highlighted in orange in Figure 3b.

Finally, auxiliary edges manage the overall flow of pods within the network. Source-to-Standby edges connect the source vertex to the standby vertices at $t = 0$. They represent the initial availability of pods in the system. Each such edge has a cost of c^{fleet} . Sink-to-Standby edges connect the standby vertices at T_{max} to the sink vertex. They represent pods concluding their journey within the planning horizon. Each such arc has a cost of zero. A Sink-to-Source edge then closes the circulation, connecting the Sink Vertex back to the Source Vertex, with a cost of zero.

The minimum cost circulation in network G represents the solution to our optimization problem. The flow value corresponds to the optimal fleet size. To extract the individual pod routes, we recursively trace a directed path from S to T , and then remove that path from the flow network. The time-space network can be reduced in size without affecting the final solution to the optimization problem. Each pod route connects its Requester Vertex to its Releaser Vertex through Middle Vertices. Since these Middle Vertices serve as intermediate points on an already defined and zero-cost in-service path, and do not represent decision points, costs, or capacities that affect the optimization, they can be bypassed. Consequently, all Middle Vertices and their incident edges can be removed. This results in a Requester Vertex and a Releaser Vertex without any edge in between.

For this reduced network, the number of vertices is given by $2|\mathbf{R}| + |\mathbf{S}| \cdot |\mathbf{T}| + 2$. Here, $2|\mathbf{R}|$ accounts for one Requester and one Releaser vertex for each pod route, $|\mathbf{S}| \cdot |\mathbf{T}|$ represents the number of Standby vertices, and

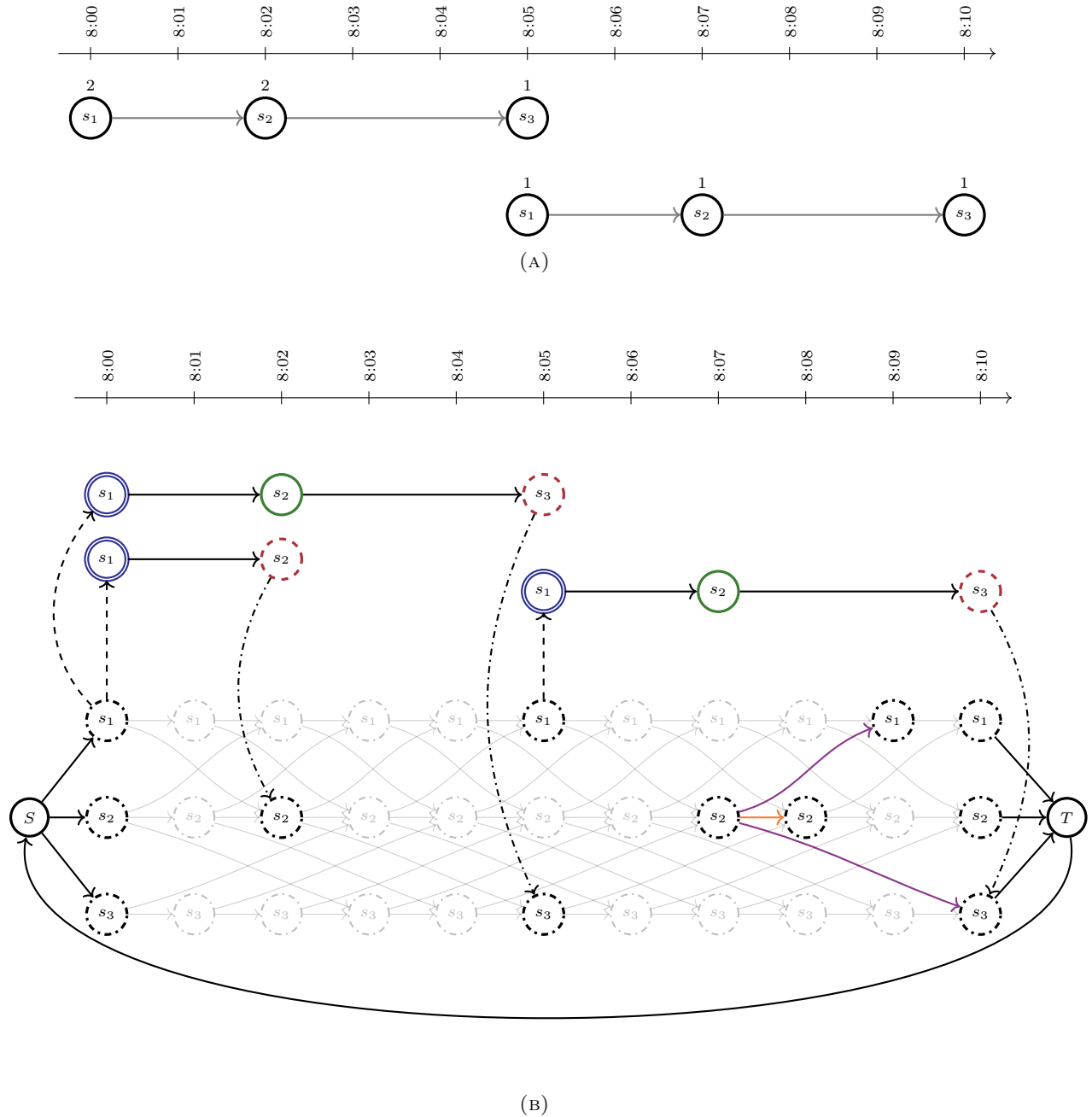


FIGURE 3. (a) Illustration of a bus schedule with two bus runs. The minimum number of required pods for each demand node is indicated above the node. (b) Time-space network of the bus schedule in Figure 3a. Vertices are shown as Requester (solid double blue); Middle (solid green); Standby (dashed-dot); S (Source); and T (Sink). Edges are represented by Standby-to-Requester (dashed lines); Releaser-to-Standby (dashed-dot lines); Standby-to-Standby parking (solid orange); and Standby-to-Standby movement (solid purple). $\Delta t = 1$ minute.

2 accounts for the source and sink vertices. The number of edges in this reduced network is approximated by $2|\mathbf{S}| + |\mathbf{S}|^2 \cdot (|\mathbf{T}| - 1) + 2|\mathbf{R}| + 1$. This includes $2|\mathbf{S}|$ for edges connecting the source and sink vertices to the initial and final standby vertices, $|\mathbf{S}|^2 \cdot (|\mathbf{T}| - 1)$ for the maximum number of edges between Standby vertices, $2|\mathbf{R}|$ for edges connecting pod routes to standby vertices via their Requester and Releaser points, and one edge for the Sink-to-Source circulation loop.

4.2. Hierarchical Pod Routing. The Hierarchical Pod Routing approach addresses the modular pod rebalancing problem through a two-stage optimization process. This strategy prioritizes the determination of the minimum required fleet size before optimizing the details of individual pod movements. In the first stage, the minimum number of pods necessary to cover all scheduled trips and their high-level assignments to specific bus runs are identified. Subsequently, the second stage focuses on optimizing the detailed routes for these assigned pods. This optimization specifically considers parking and empty movement costs incurred during the between-service periods.

4.2.1. Stage 1: Minimum Fleet Size Determination. The first stage of the Hierarchical Pod Routing approach focuses on determining the minimum fleet size required to cover all scheduled bus runs. This is achieved by formulating the problem as a Minimum Disjoint Path Cover on a Directed Acyclic Graph (DAG). The following paragraphs provide the details of the construction of this DAG and explain how its solution yields the optimal number of pods needed for in-service operations.

The graph for this stage, denoted as H , utilizes the concepts of Requester, Middle, and Releaser vertices defined in Section 4.1. While the Middle vertices are included in the graph, it will be demonstrated later that they can be removed without impacting the final solution.

Pods departing from Releaser vertices are empty and thus available to serve other demand points that require an empty pod. An edge is therefore established from any Releaser vertex (e.g., representing the end of pod route r_1) to any Requester vertex (e.g., representing the start of pod route r_2) if the continuous travel time from $End(r_1)$ to $Start(r_2)$ ($\tau_{End(r_1), Start(r_2)}$) does not exceed the time difference between their continuous scheduled service times ($StartTime_{r_2} - EndTime_{r_1}$). The graph constructed using this approach from the bus runs of Figure 2 is presented in Figure 4. We claim that network H is a DAG, and that the minimum fleet size that addresses the demand corresponds to the minimum number of paths that cover all nodes in network H without sharing any nodes.

Theorem 2. *Network H is a DAG.*

Proof. To prove that network H is acyclic, we examine the structure of its edges. Edges originating from requester and middle nodes can only connect to other nodes within the same bus run. A directed cycle involving requester and middle nodes would imply that pods are able to travel backward in time, which is physically impossible. Consequently, the only remaining possibility would be the existence of a cycle composed solely of releaser nodes. However, since there are no edges between releaser nodes, such a cycle cannot exist. Therefore, network H does not contain any directed cycles, and it is, therefore, a DAG. \square

Minimizing the fleet size in the transit network directly translates into finding the minimum disjoint path cover on graph H . In this context, every path represents the complete journey of a single pod. Our objective, therefore, is to find the smallest group of these paths, each representing a distinct pod's journey. This group must cover every demand node exactly once, and its paths must be disjoint, meaning no two pods overlap on any service task. The edges of the graph guarantee that any constructed path represents a physically feasible sequence of service for a pod within the transit network.

While finding the minimum disjoint path cover in an arbitrary graph is NP-hard (Franzblau and Raychaudhuri, 2002), the problem simplifies to a maximum matching problem in DAGs (Fulkerson, 1956). This allows the solution to be computed in polynomial time. To find a minimum disjoint path cover in a DAG $H = (V, E)$, we adopt the method described by Bertossi et al. (1987). The approach constructs a bipartite graph by replacing each vertex $v \in V$ with two vertices v' and v'' . For every edge $(v_i, v_j) \in E$ in the original DAG, an undirected edge is added between v_i'' and v_j' in the bipartite graph. A maximum matching is then computed in this bipartite graph. The number of vertex-disjoint paths required to cover all nodes in the original DAG corresponds to the number of unmatched nodes in the matching. An illustration of this transformation is provided in Figure 5.

The structure of graph H makes it unnecessary to double the number of nodes, as is required by the bipartite transformation. It also enables a reduction in the graph size before solving the matching problem. Specifically, any path in a minimum disjoint path cover that includes a requester node must inevitably pass through all its middle nodes and reach the corresponding releaser node; otherwise, the path cover would not be minimum. As a result, the requester node alone is sufficient to determine the sequence of remaining nodes in the path. A modified version of H is obtained by removing all middle nodes and all edges that directly connect a requester node to its corresponding releaser node. The remaining directed edges are then replaced with undirected edges. The resulting graph is bipartite, with requester nodes in one partition and releaser nodes in the other. A maximum

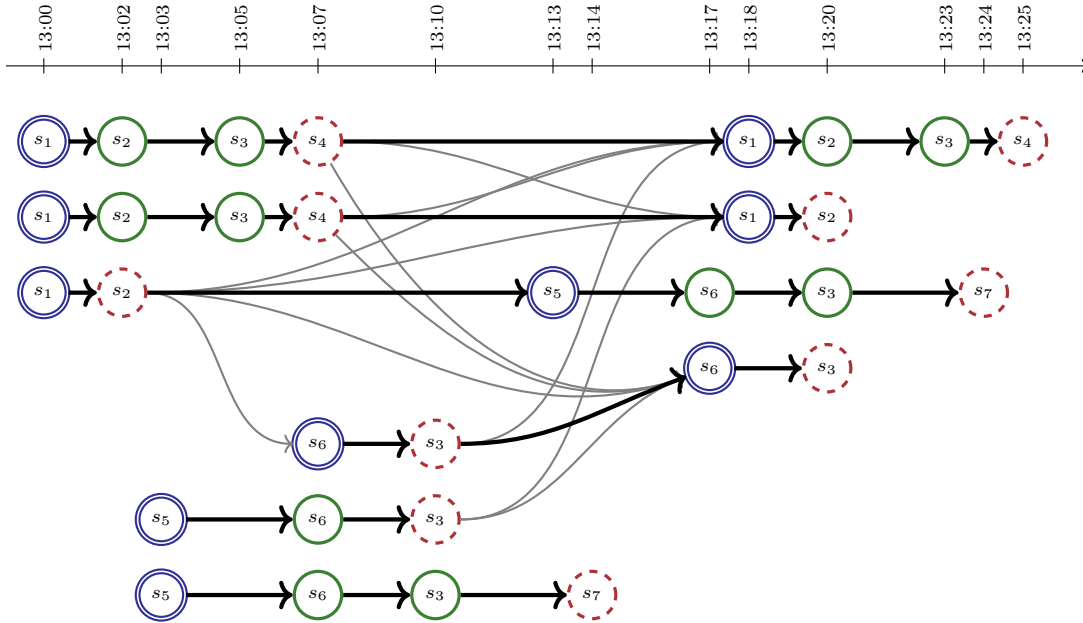


FIGURE 4. Graph H representing the bus transit schedule in Figure 2. Edges indicate feasible pod transitions. The minimum disjoint path cover is emphasized with thick black lines.

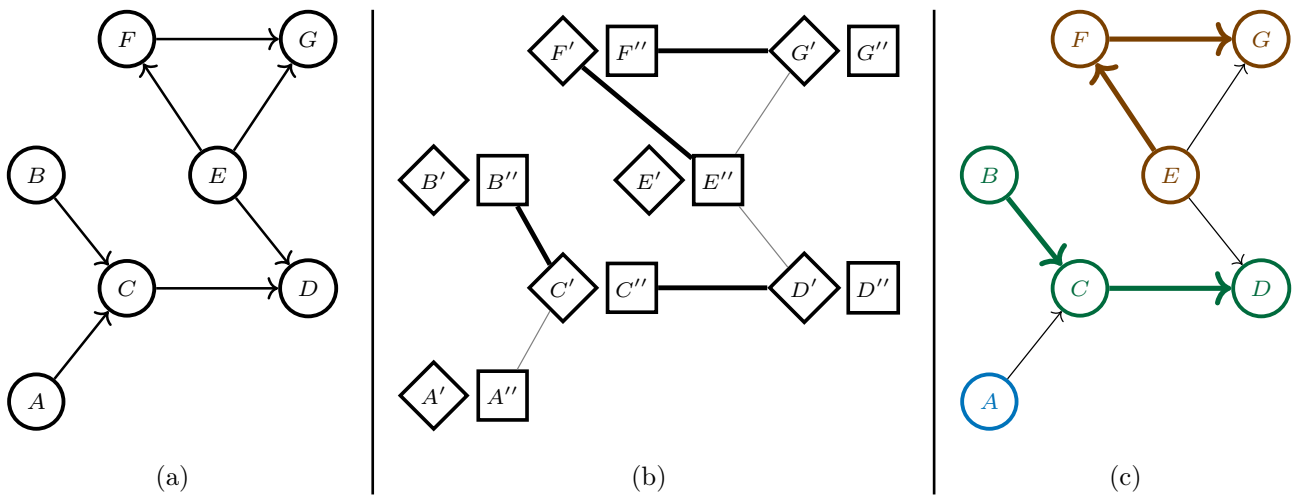


FIGURE 5. (a) The input DAG. (b) Bipartite transformation with bold edges forming a maximum matching. (c) Minimum path cover: $A; B \rightarrow C \rightarrow D$; and $E \rightarrow F \rightarrow G$.

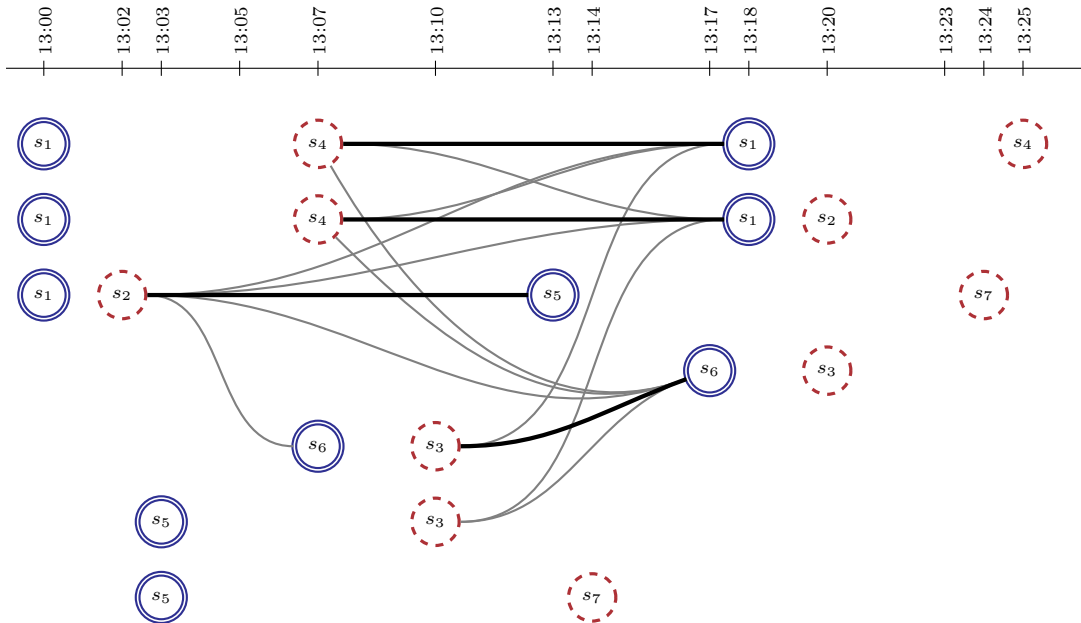


FIGURE 6. Bipartite graph obtained by removing all middle nodes and requester-to-releaser edges from the graph in Figure 4, and replacing the remaining directed edges with undirected edges. The maximum matching is shown with bold edges.

matching in this bipartite graph can then be used to reconstruct the minimum disjoint path cover in the original network. Figure 6 shows the bipartite graph obtained by removing all middle nodes and all requester-to-releaser edges from the graph in Figure 4.

For this bipartite graph, the number of nodes is $2|\mathbf{R}|$, representing one Requester node and one Releaser node for each pod route. The number of edges is approximated for a bus schedule where bus runs are uniformly distributed across the service time. In such a scenario, the number of edges can be estimated by:

$$\int_0^{T_{\max}} \frac{T_{\max} - t}{T_{\max}} |\mathbf{R}| \cdot \frac{|\mathbf{R}|}{T_{\max}} dt = \frac{|\mathbf{R}|^2}{2} \quad (13)$$

Here, $\frac{|\mathbf{R}|}{T_{\max}} dt$ represents the approximate number of Releaser nodes within a small time interval dt around time t , and $\frac{T_{\max} - t}{T_{\max}} |\mathbf{R}|$ represents the approximate number of Requester nodes available after time t that a Releaser node at time t could potentially connect to. Since the graph size is a polynomial factor of the number of bus runs, finding the minimum fleet size can be done in polynomial time.

4.2.2. Stage 2: Between-Service Routing. The output from Stage 1 provides a sequence of in-service pod routes assigned to each pod. However, the precise routing of these pods during the intervals between their assigned pod routes remains unspecified. To address this challenge, the methodology from the Integrated Pod Routing approach is adapted. For each pod and for each interval between its assigned in-service pod routes, a dedicated time-space network is created. The optimal routing for the pod within that interval is then determined by solving a minimum-cost flow problem on this localized network.

The routing within each interval for a pod falls into one of three distinct categories. (a) This occurs when a pod is available and the overall service period has begun, but it remains unassigned to any specific pod route (Figure 7a); (b) This covers situations where a pod completes one assigned pod route and is then assigned to begin another (Figure 7b); or (c) This involves a pod that has finished its last assigned pod route but remains in the system before the overall service period concludes (Figure 7c).

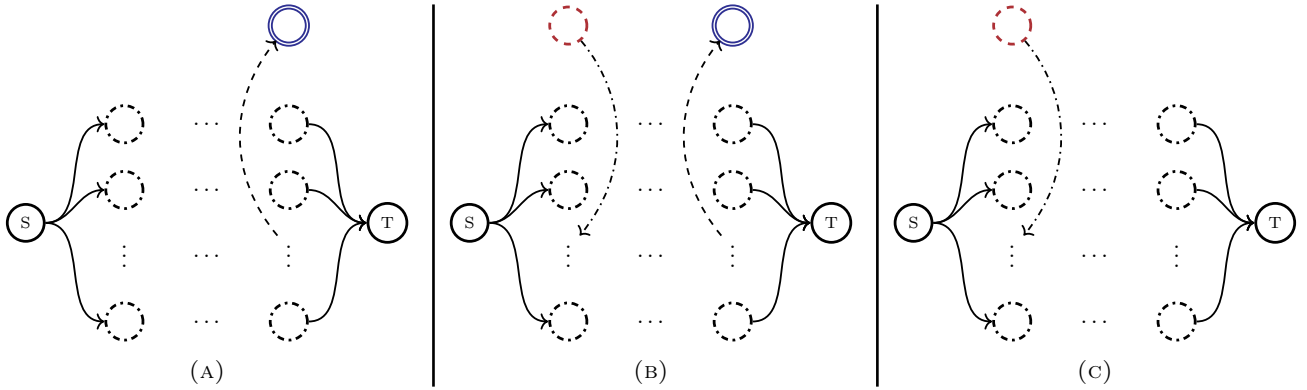


FIGURE 7. Three categories of routing for a pod within an interval: (a) pod available but unassigned; (b) pod transitioning between assigned routes; (c) pod remaining in system after its last assigned route concludes.

Edge definitions and associated costs for these localized time-space networks are consistent with Section 4.1, except for a key difference concerning the fleet cost. This cost is included for networks of the first routing category (Category a). It is not included for networks of the second (Category b) and third (Category c) routing categories. This is due to the fact that the pod is already part of an ongoing assignment chain in these cases.

In cases where an assignment interval is long, its corresponding time-space network may grow to a size comparable to the full integrated network. In such scenarios, the hierarchical method may lose its computational advantage, as the resulting subproblems remain large and memory-intensive, and must be solved multiple times rather than once. To address this issue, a refined approach, called Hierarchical-Capped, is introduced. The method introduces a user-defined cap on the duration of each assignment interval, selected based on the available computational resources. This cap helps manage the size of the time-space network, which grows linearly with the interval duration. When an interval exceeds the specified threshold, it is divided into smaller subintervals that are solved sequentially. Because the flow value in each interval is known to be exactly one unit (representing a single pod), the interval can be safely divided into smaller subintervals without risking unserved demand. After solving the flow for one subinterval, the station that receives the pod at the end becomes the starting point for the next subinterval. This sequential structure preserves flow continuity while allowing smaller networks to be solved independently, significantly reducing memory and computation requirements. It is important to note that, while the Hierarchical-Capped approach mitigates computational challenges, it may yield suboptimal solutions compared to the original Hierarchical approach. Therefore, it was used only when it was deemed necessary due to computational constraints.

5. CASE STUDY

This section presents a detailed case study to evaluate the proposed modular pod rebalancing models under realistic demand. The study focuses on local bus routes within the borough of Manhattan in New York City. The subsequent subsections detail the data collection process, model implementation, and scenario definitions.

5.1. Data Collection and Preparation. New York City’s public transit system, operated by the Metropolitan Transportation Authority (MTA), offers extensive data resources relevant to this study. In 2023, the MTA bus network recorded an average daily ridership of approximately 1.4 million passengers (Metropolitan Transportation Authority, 2024). This study utilizes static and real-time General Transit Feed Specification (GTFS) data from the MTA to perform a detailed analysis. Static GTFS data includes comprehensive information on routes and scheduled service times. The investigation focuses on local bus routes operating within the borough of Manhattan during weekdays, covering 41 distinct routes and a total of 24,693 weekday bus runs. Figure 8a illustrates the number of active bus runs throughout the day.

To supplement the static data, GTFS real-time API requests were sent every minute on February 7 and 14, as well as from February 17 to 21 and 24 to 28, 2025. These requests captured live snapshots of buses operating in the system at those moments. Some of the responses included onboard passenger counts.

At the end of the data collection process, each GTFS real-time record was matched to its corresponding scheduled bus run and stop sequence. Since real-time snapshots are often captured while buses are traveling between stops, the onboard passenger count at that moment provides a lower bound for both the preceding stop and the upcoming stop. After associating passenger counts with their respective trips for each day, the data from all collection days were combined. Assuming similar passenger demand on weekdays, the number of passengers at each stop was estimated as the maximum observed value across all days. This approach provides a conservative estimate of passenger volume at each stop.

Despite the matching process, 40.1% of the trips had no stops with any passenger count data. These trips were excluded and the analysis focused on those with at least some passenger count data. Of the remaining 59.9%, passenger counts were available for approximately 62.6% of stops. For the remaining stops without data, the passenger count was estimated by taking the maximum of the counts from the nearest preceding or following stop with an available passenger count. Figure 8b shows the average onboard occupancy throughout the day, based on both real-time observations and estimated values for missing stops. The average bus occupancy across all observations was approximately 19%. Assuming that each pod has a capacity of 16 passengers (Sustainable Bus, 2024), the number of pods required at each stop can be calculated.

5.2. Experimental Design. To evaluate how memory usage and solution quality vary with network size for both solution approaches, 15 subsets of bus runs were selected from the bus system in Manhattan. Each subset includes bus runs that collectively cover a specific number of stations, allowing controlled variation in network size. For each subset, both the time-space network G and the corresponding bipartite graph H were constructed. The number of edges in these networks is reported in Table 2. To examine the impact of temporal resolution, four different time steps ($\Delta t = 5, 15, 30,$ and 60 seconds) were created for network G .

As shown in Table 2, the number of stations in the selected subsets varies from 13 to 240, which results in significant differences in the scale of network G . Network G becomes larger as the number of stations grows and the temporal resolution becomes finer. In contrast, the size of network H depends more on the number of bus runs, as its structure reflects possible connections between pod routes.

To define the cost parameters for a realistic cost scenario, several assumptions were made based on current transportation trends. For the fleet cost of a pod, c^{fleet} , it was assumed that the purchase price of an electric pod is comparable to that of an autonomous electric vehicle. A purchase price of 40,000 USD and a life expectancy of 8 years yield a daily cost of approximately 13.7 USD per pod. This number is aligned with the capital cost

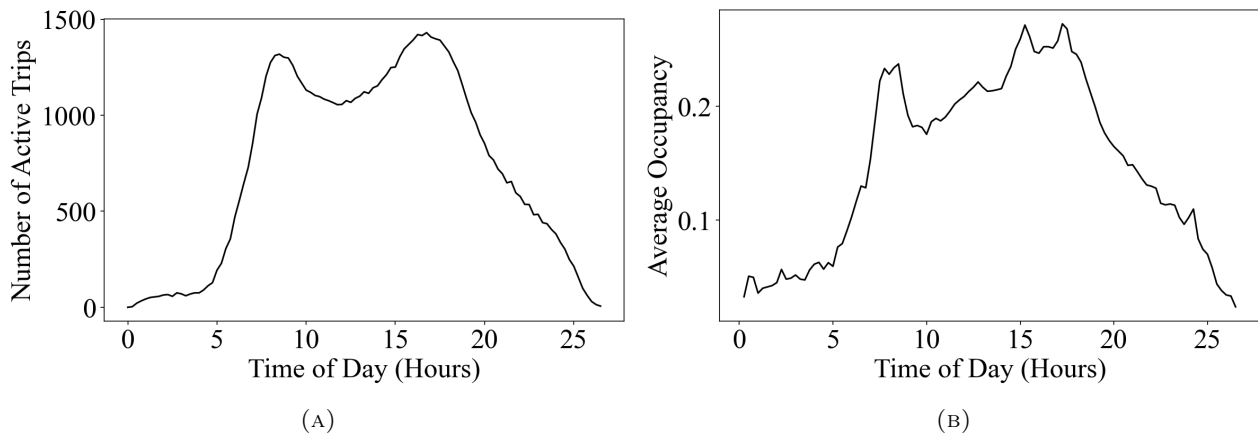


FIGURE 8. (a) Number of active bus runs throughout a weekday day. (b) Average bus occupancy over the day, combining real-time observations and estimated values.

TABLE 2. Edge counts for networks G and H across all instances and time steps.

Instance	# Stations	# Bus Runs	G				H
			Δt (s)	5	15	30	60
1	13	309	2,905,895	969,691	485,647	243,541	235,799
2	13	312	2,922,465	975,259	488,463	245,059	283,349
3	14	122	2,840,019	947,005	473,759	237,137	17,303
4	14	260	3,320,137	1,107,745	554,651	278,107	238,936
5	14	338	3,462,327	1,155,437	578,709	290,351	411,007
6	15	261	3,811,125	1,271,447	636,539	319,092	262,148
7	20	489	6,898,207	2,301,009	1,151,709	577,073	572,079
8	30	244	13,330,097	4,444,221	2,222,761	1,112,043	77,748
9	41	678	23,065,481	7,692,695	3,849,529	1,927,905	3,209,093
10	59	86	43,173,838	14,392,742	7,197,475	3,599,810	10,726
11	72	354	72,965,191	24,669,192	12,336,803	6,170,621	337,336
12	91	154	141,201,381	47,597,520	23,801,253	11,903,184	65,847
13	100	379	182,953,259	60,987,693	30,809,771	15,408,419	354,997
14	184	328	620,594,015	205,746,093	103,448,016	26,340,525	330,592
15	240	410	886,507,566	296,774,737	148,403,510	37,472,615	969,840

of the pod in Cheng et al. (2024). The cost of empty movement, c^{move} , was based on an energy consumption of 1 KWH/mile, an average speed of 15 mph, and an electricity price of 0.13 USD/KWH, resulting in a cost of approximately 0.03 USD per minute. The magnitude of this cost aligns with the energy cost of the pod presented in Cheng et al. (2024) as well as Romea and Estrada (2021). Finally, the parking cost, c_s^{Park} , was set at 2 USD per hour, which is approximately 0.03 USD per minute.

Beyond the realistic cost configuration, several alternative cost scenarios are explored. In one scenario, only the fleet cost of each pod is considered, with all other costs set to zero. Under this setup, the Hierarchical method produces the exact minimum fleet size, which serves as a baseline for comparing the solution quality of the Integrated Pod Routing approach at different time steps. Another scenario excludes the fleet cost and focuses solely on minimizing parking and empty movement costs. Additional scenario considers zero empty movement cost to isolate the impact of parking cost. Finally, a scenario introduces variability in parking prices, where the parking cost c_s^{Park} is selected uniformly at random from the set $\{0.01, 0.02, 0.03, 0.04, 0.05, 0.06, 0.07, 0.08\}$ USD per minute. Table 3 summarizes the full set of cost scenarios considered in the analysis.

TABLE 3. Cost Configurations

Scenario	c^{fleet}	c^{move}	c_s^{Park}
S1: Baseline (All Costs)	13.7	0.03	0.03
S2: Fleet Cost Only	13.7	0	0
S3: No Fleet Cost	0	0.03	0.03
S4: No Movement Cost	13.7	0	0.03
S5: Variable Parking Cost	13.7	0.03	Uniform from $\{0.01, 0.02, \dots, 0.08\}$

5.3. Computational Details and System Configuration. This section describes the hardware, software, and solvers used to implement and run the optimization models.

The minimum-cost flow problems formulated on the time-space networks are solved using the Gurobi Optimizer. The models are implemented in Python using the Gurobi Python API. Computational experiments are conducted on a Google Cloud Platform virtual machine instance. Specifically, the instance is of type `c2d-highmem-112`, featuring 112 vCPUs and 896 GB of memory. The system architecture is `x86_64`, running Debian GNU/Linux 12 (Bookworm). During optimization, the Gurobi network simplex algorithm is applied.

To solve the maximum matching problems on bipartite graphs, a GPU-based push-relabel algorithm with global relabeling is employed (Deveci et al., 2013). The implementation is adapted from code provided by the

authors in a publicly available CUDA repository². Computations are conducted on a dedicated Google Cloud VM of type `g2-standard-32`, equipped with 32 vCPUs, 125 GB of RAM, and an NVIDIA L4 GPU with 24 GB of memory. The system operates on Debian GNU/Linux 11 (Bullseye) with CUDA version 12.4 and NVIDIA driver version 550.90.07.

6. RESULTS AND DISCUSSION

This section presents the results obtained from applying the proposed routing approaches to the case study described in Section 5.1. The analysis covers the various network instances and cost scenarios defined in Section 5.2. Solution quality and computational efficiency are discussed across different network scales and temporal resolutions.

6.1. Solution Performance. Table 4 summarizes the objective function values obtained from the Integrated and Hierarchical Pod Routing methods for Scenario 1 (Baseline) across the first 13 instances. Instances 14 and 15 are designed specifically for the Hierarchical-Capped method and are excluded from this comparison. The results for Integrated Pod Routing are presented for four discrete time steps: 5, 15, 30, and 60 seconds, while the Hierarchical Pod Routing uses a fixed 30-second resolution for Stage 2.

Across all 13 instances, reducing the time step from 30 to 5 seconds in the Integrated method does not improve the objective function values. In contrast, increasing the time step to 60 seconds occasionally results in a higher objective, as observed in Scenario 2. These results suggest that a 30-second resolution is sufficient for capturing the necessary temporal detail. Finer resolutions increase network size and computational complexity without yielding better solutions. This observation aligns with practical considerations, since scheduling at very fine intervals does not reflect the inherent imprecision in real-world operations.

In this cost scenario, the Hierarchical method performs at least as well as the Integrated method in terms of objective value, and in some instances, it produces slightly better results. This is because Stage 1 in the hierarchical approach operates in continuous time, and an edge is added between a releaser and a requester node whenever a pod can reach the requester within the required time window. In contrast, the Integrated method uses discrete time and involves two additional steps: the pod must first move to a standby node after release and later be reassigned from a standby node to the requester. Each of these steps can introduce a delay of up to Δt , which may cause some transitions that are feasible in the hierarchical method to become infeasible in the integrated method.

Table 5 compares the objective values of the two solution approaches under the remaining cost scenarios. For all scenarios, the time-space networks are constructed with a temporal resolution of $\Delta t = 30$ seconds. In Scenario 2

TABLE 4. Comparison of Objective Values for Integrated and Hierarchical Pod Routing. Bold values indicate lower objective function values between the two methods.

Instance	Integrated				Hierarchical
	5	15	30	60	
1	1743.95	1743.89	1743.95	1800.73	1743.95
2	1992.14	1992.14	1992.14	2049.16	1992.14
3	437.89	437.89	437.89	437.89	437.89
4	1547.23	1547.23	1547.23	1547.23	1435.49
5	2666.02	2666.02	2666.02	2666.02	2666.02
6	1654.98	1654.98	1654.98	1654.98	1599.37
7	2691.96	2691.96	2691.96	2691.96	2691.96
8	1038.32	1038.32	1038.32	1038.32	1038.32
9	7956.34	7956.34	7956.34	8150.10	7723.90
10	570.57	570.57	570.55	570.57	526.36
11	1697.76	1697.76	1697.76	1697.76	1649.23
12	1660.66	1660.66	1660.66	1717.77	1660.66
13	4806.67	4806.67	4806.68	4806.67	4749.93

²<https://github.com/nagendervss/BipartiteMatchingCUDA>

(Fleet Cost Only), the objective includes only the cost of purchasing pods. As a result, minimizing the total cost reduces to minimizing the fleet size. The Hierarchical method solves this in Stage 1 using an exact algorithm. It therefore produces exact solutions in this scenario, whereas the integrated method yields approximate ones. The average percentage error in pod size is approximately 1.67%, indicating that the Integrated Pod Routing method provides reasonably accurate estimates.

Scenario 3 (No Fleet Cost) shows that the hierarchical method continues to outperform the integrated method, even when the fleet cost is removed from the objective function. Parking and empty movement costs remain part of the cost structure, so pods that are not serving still contribute to the total cost. Consequently, reducing the number of pods remains an effective strategy for minimizing total system cost. This outcome depends on the relative cost structure. For instance, if parking were significantly cheaper than empty movement, it might be more cost-effective to introduce additional pods to serve local demand. These pods could then park immediately, rather than moving across the network to serve other requests. Scenario 4 (No Movement Cost) examine cases where empty movement cost is significantly higher than the parking cost, while fleet cost is still included in the objective. These results show that the hierarchical method continues to outperform the integrated method in most instances.

For Scenario 5 (Random Parking), both the Integrated and Hierarchical methods produce comparable solutions. When the Integrated method yields a lower objective value, the average relative gap is approximately 0.79%. In contrast, when the Hierarchical method provides the better solution, the average relative gap rises to 2.92%, indicating a more substantial advantage in those cases.

6.2. Computational Performance. Stage 1 of the hierarchical method is solved efficiently using the GPU-based maximum matching algorithm. The solve time ranges from 0.224 to 0.267 seconds across all instances and shows efficient performance.

The most computationally demanding step in both methods is solving the minimum cost flow on the time-space network. In the integrated method, the entire service horizon is modeled as a single network, resulting in one large optimization problem. In contrast, the hierarchical method breaks the problem into smaller intervals and solves separate time-space networks for each. Solution time and peak memory usage were monitored during the implementation of the integrated algorithm across all instances. As shown in Figures 10a and 10b, both metrics grow super-linearly with the number of edges in the network. This scaling behavior implies that smaller time-space networks are computationally more efficient. Extrapolating from these results, optimizing pod allocations for the full Manhattan network would require approximately 3 TB of RAM and 36 hours of computation.

For the hierarchical pod routing method, memory efficiency depends on the duration of the scheduling intervals. Table 6 summarizes these durations, and Figure 9 illustrates their distribution. While repositioning

TABLE 5. Objective Function Comparison Across Cost Scenarios. Bold values indicate lower objective function values between the two methods.

Instance	S2		S3		S4		S5	
	Integrated	Hierarchal	Integrated	Hierarchal	Integrated	Hierarchal	Integrated	Hierarchal
1	506.90	506.90	1237.05	1237.05	510.64	510.64	1023.27	1021.47
2	589.10	589.10	1403.04	1403.04	593.12	593.12	1180.15	1181.93
3	150.70	150.70	287.19	287.19	151.39	151.38	275.24	274.92
4	465.80	438.40	1081.43	997.09	471.19	443.78	942.74	889.38
5	739.80	739.80	1926.22	1926.22	747.40	747.38	1529.84	1537.1
6	493.20	479.50	1161.78	1119.87	498.54	484.83	994.18	962.56
7	767.20	767.20	1924.76	1924.76	771.92	771.96	1562.98	1572.3
8	342.50	342.50	695.82	695.82	343.90	343.94	596.29	610.32
9	3096.20	3027.70	4860.14	4696.20	3115.80	3047.41	4975.25	5058.24
10	205.50	191.80	365.07	334.56	206.21	192.51	349.89	327.96
11	616.50	602.80	1081.26	1046.43	620.59	606.89	1039.50	1041.54
12	493.20	493.20	1167.46	1167.46	496.02	496.02	976.23	977.24
13	1438.50	1424.80	3368.18	3325.13	1443.59	1424.80	2940.39	2903.76

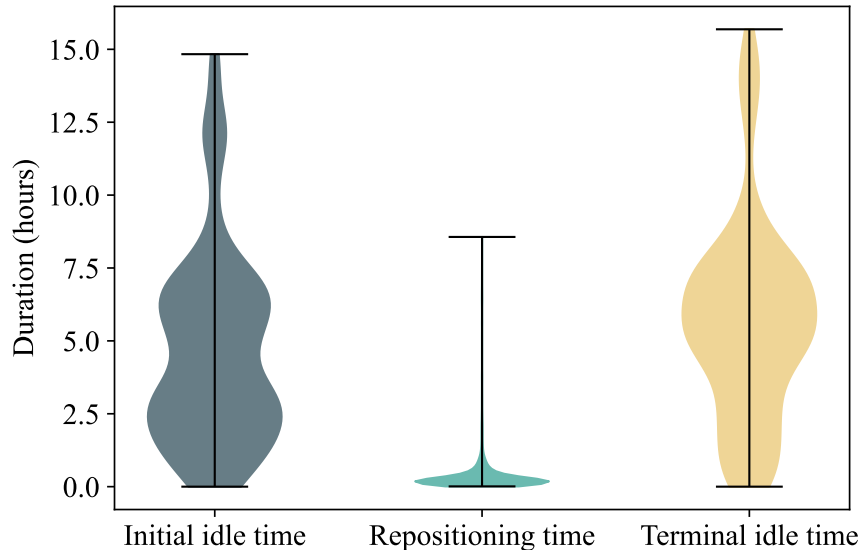


FIGURE 9. Distribution of interval durations in the hierarchical method.

intervals are typically short, initial and terminal idle periods can be substantially longer. These long intervals can significantly expand the size of the corresponding time-space networks. As a result, the required memory may become comparable to that of solving the full integrated network in a single run.

Table 7 shows the results for Instances 12–15 using the Hierarchical-Capped method. The method sets a cap on the time-space network size to reduce memory use and solve instances that require high memory and long runtimes under the original Hierarchical method. In these cases, the maximum number of nodes in each subinterval is set to approximately 15,000. Although the Capped approach is heuristic, the objective values stay close to those of the Integrated method. In all cases, the gap is small, and the method provides a practical option when computational limits make the original model difficult to solve.

7. CONCLUSIONS

This study addresses the challenge of rebalancing empty modular transit vehicles between fixed-service schedules. Unlike existing approaches that focus primarily on in-service operations, the proposed framework explicitly models between-service repositioning, accounting for pod acquisition, maintenance, parking, and movement costs. The proposed two-stage hierarchical method first determines the minimum fleet size via a GPU-accelerated maximum matching algorithm, then generates detailed routing plans through a sequence of minimum-cost flow problems on time-space networks. To address excessive computational memory demands in large instances, a capped-interval heuristic was introduced. This limits the size of each subproblem and makes computation tractable.

Experiments on a large-scale Manhattan bus network show that the hierarchical method achieves objective values on par with or better than the full-scale integrated formulation, while requiring significantly less memory.

TABLE 6. Descriptive statistics of interval durations (hours).

Interval Type	Mean	Std	Min	25%	50%	75%	Max
Initial idle time	4.65	3.32	0.00	2.07	4.18	6.58	14.83
Repositioning time	0.40	0.77	0.01	0.13	0.20	0.34	8.56
Terminal idle time	5.61	3.50	0.00	3.18	5.44	7.25	15.69

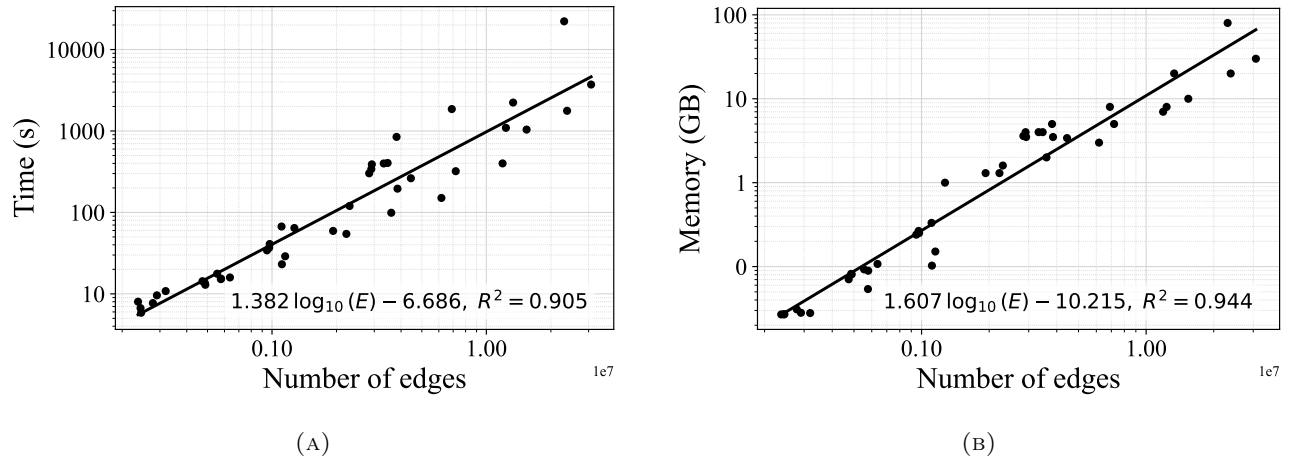


FIGURE 10. Log-log scatter plots with fitted power-law lines and R^2 annotations. (a) Total solve time vs. number of edges. (b) Memory usage vs. number of edges.

TABLE 7. Comparison of objective value and memory usage across Integrated vs. Hierarchical-Capped methods

Instance	Integrated		Hierarchical-Capped	
	Obj	Memory (GB)	Obj	Memory (GB)
12	976.23	17.95	986.8	6.33
13	2940.39	21.10	2959.20	16.87
14	1580.65	257.33	1529.97	89.66
15	4320.69	563.24	4280.35	121.47

This improvement in memory efficiency enables the proposed method to scale to large networks that are otherwise computationally infeasible to solve using a single integrated network.

It is important to note that while Algorithm 1(DECOMPOSE_BUS_RUN) identifies the minimum number of pod routes to satisfy the demand for in-service routing, the configuration of pod routes can influence the between-service routing. In the ideal situation, the in-service and between-service routing should be jointly optimized. Such a joint optimization, however, is beyond the scope of this study and is left for future research. Furthermore, future work can extend this framework to incorporate stochastic demand patterns and stochastic travel times, allowing the model to better reflect real-world variability.

DECLARATION OF GENERATIVE AI AND AI-ASSISTED TECHNOLOGIES IN THE WRITING PROCESS

The authors acknowledge the use of AI-assisted tools (such as ChatGPT and Gemini) for language editing and grammar refinement during manuscript preparation. No AI tool was used for generating novel content, data analysis, or drawing conclusions. All responsibility for the accuracy and integrity of the manuscript remains with the authors.

DECLARATION OF CONFLICTING INTEREST

The authors declared no potential conflicts of interest with respect to the research, authorship, and/or publication of this article.

REFERENCES

- Bel, G. and Holst, M. (2018). Evaluation of the impact of bus rapid transit on air pollution in Mexico City. *Transport Policy*, 63:209–220.
- Bertossi, A. A., Carraresi, P., and Gallo, G. (1987). On some matching problems arising in vehicle scheduling models. *Networks*, 17(3):271–281.
- Cao, H. and Zhao, J. (2025). Optimizing modular vehicle public transportation services with short-turning strategy and decoupling/coupling operations. *Sustainability*, 17(3):870.
- Ceder, A. and Stern, H. I. (1981). Deficit function bus scheduling with deadheading trip insertions for fleet size reduction. *Transportation Science*, 15(4):338–363.
- Chen, Z. and Li, X. (2021). Designing corridor systems with modular autonomous vehicles enabling station-wise docking: Discrete modeling method. *Transportation Research Part E: Logistics and Transportation Review*, 152:102388.
- Chen, Z., Li, X., and Zhou, X. (2019). Operational design for shuttle systems with modular vehicles under oversaturated traffic: Discrete modeling method. *Transportation Research Part B: Methodological*, 122:1–19.
- Cheng, X., Nie, Y. M., and Lin, J. (2024). An autonomous modular public transit service. *Transportation Research Part C: Emerging Technologies*, 168:104746.
- Cortés, C. E., Jara-Díaz, S., and Tirachini, A. (2011). Integrating short turning and deadheading in the optimization of transit services. *Transportation Research Part A: Policy and Practice*, 45(5):419–434.
- Dai, Z., Liu, X. C., Chen, X., and Ma, X. (2020). Joint optimization of scheduling and capacity for mixed traffic with autonomous and human-driven buses: A dynamic programming approach. *Transportation Research Part C: Emerging Technologies*, 114:598–619.
- Dakic, I., Yang, K., Menendez, M., and Chow, J. Y. (2021). On the design of an optimal flexible bus dispatching system with modular bus units: Using the three-dimensional macroscopic fundamental diagram. *Transportation Research Part B: Methodological*, 148:38–59.
- Deveci, M., Kaya, K., Ucar, B., and Çatalyürek, Ü. V. (2013). A push-relabel-based maximum cardinality bipartite matching algorithm on GPUs. In *2013 42nd International Conference on Parallel Processing*, pages 21–29.
- Ford, L. R. and Fulkerson, D. R. (2015). *Flows in Networks*. Princeton University Press, Princeton, NJ.
- Franzblau, D. S. and Raychaudhuri, A. (2002). Optimal hamiltonian completions and path covers for trees, and a reduction to maximum flow. *The ANZIAM Journal*, 44(2):193–204.
- Fulkerson, D. R. (1956). Note on Dilworth’s decomposition theorem for partially ordered sets. *Proceedings of the American Mathematical Society*, 7(4):701–702.
- Gintner, V., Kliwer, N., and Suhl, L. (2005). Solving large multiple-depot multiple-vehicle-type bus scheduling problems in practice. *Or Spectrum*, 27(4):507–523.
- Ha, J., Lee, S., and Ko, J. (2020). Unraveling the impact of travel time, cost, and transit burdens on commute mode choice for different income and age groups. *Transportation Research Part A: Policy and Practice*, 141:147–166.
- Khan, Z. S., He, W., and Menéndez, M. (2023). Application of modular vehicle technology to mitigate bus bunching. *Transportation Research Part C: Emerging Technologies*, 146:103953.
- Khan, Z. S. and Menéndez, M. (2023). Bus splitting and bus holding: A new strategy using autonomous modular buses for preventing bus bunching. *Transportation Research Part A: Policy and Practice*, 177:103825.
- Khan, Z. S. and Menéndez, M. (2025). No time for stopping: A stop-less autonomous modular (slam) bus service. *Transportation Research Part C: Emerging Technologies*, 171:104888.
- Kliwer, N., Mellouli, T., and Suhl, L. (2006). A time-space network based exact optimization model for multi-depot bus scheduling. *European Journal of Operational Research*, 175(3):1616–1627.
- Liu, T., Ceder, A., and Rau, A. (2020). Using deficit function to determine the minimum fleet size of an autonomous modular public transit system. *Transportation Research Record*, 2674(11):532–541.
- Metropolitan Transportation Authority (2024). About the MTA. <https://www.mta.info/about>. Accessed: 2025-06-02.
- Muñoz, J. C. (2002). *Driver-shift design for single-hub transit systems under uncertainty*. University of California, Berkeley.

- Olsen, N., Kliewer, N., and Wolbeck, L. (2022). A study on flow decomposition methods for scheduling of electric buses in public transport based on aggregated time–space network models. *Central European Journal of Operations Research*, 30(3):883–919.
- Pei, M., Lin, P., Du, J., Li, X., and Chen, Z. (2021). Vehicle dispatching in modular transit networks: A mixed-integer nonlinear programming model. *Transportation Research Part E: Logistics and Transportation Review*, 147:102240.
- Penna, P. H. V., Subramanian, A., Ochi, L. S., Vidal, T., and Prins, C. (2019). A hybrid heuristic for a broad class of vehicle routing problems with heterogeneous fleet. *Annals of Operations Research*, 273(1):5–74.
- Romea, G. and Estrada, M. (2021). Analysis of an autonomous driving modular bus system. *Transportation research procedia*, 58:181–188.
- Stopher, P. R. (2004). Reducing road congestion: a reality check. *Transport Policy*, 11(2):117–131.
- Sustainable Bus (2024). Next modular vehicle: Tecnobus unveils the 2025 pod model. <https://www.sustainable-bus.com/news/next-modular-vehicle-pod-model-2025-tecnobus-wayla/>. Accessed: 2025-06-03.
- Tian, Q., Lin, Y. H., Wang, D. Z., and Liu, Y. (2022). Planning for modular-vehicle transit service system: Model formulation and solution methods. *Transportation Research Part C: Emerging Technologies*, 138:103627.
- Tyrinopoulos, Y. and Antoniou, C. (2013). Factors affecting modal choice in urban mobility. *European Transport Research Review*, 5:27–39.
- Vazifeh, M. M., Santi, P., Resta, G., Strogatz, S. H., and Ratti, C. (2018). Addressing the minimum fleet problem in on-demand urban mobility. *Nature*, 557(7706):534–538.
- Venter, C., Jennings, G., Hidalgo, D., and Valderrama Pineda, A. F. (2018). The equity impacts of bus rapid transit: A review of the evidence and implications for sustainable transport. *International Journal of Sustainable Transportation*, 12(2):140–152.
- Wang, H. and Shen, J. (2007). Heuristic approaches for solving transit vehicle scheduling problem with route and fueling time constraints. *Applied Mathematics and Computation*, 190(2):1237–1249.
- Ye, T. and Shmoys, D. B. (2023). A min-max theorem for the minimum fleet-size problem. *Operations Research Letters*, 51(3):312–314.
- Zhan, X., Qian, X., and Ukkusuri, S. V. (2016). A graph-based approach to measuring the efficiency of an urban taxi service system. *IEEE Transactions on Intelligent Transportation Systems*, 17(9):2479–2489.